High temperature piezoelectric properties of flux-grown α-GeO 2 single crystal

Philippe Papet, Micka Bah, Abel Haidoux, Benoit Ruffle, Bertrand Ménaert, Alexandra Pena Revellez, Jérôme Debray, Pascale Armand

Journal of Applied Physics

High temperature piezoelectric properties of flux-grown α-GeO_2 single crystal

Philippe Papet[a], Micka Bah[a], Abel Haidoux[a], Benoit Ruffle[b], Bertrand Menaert[c], Alexandra Peña[c], Jérôme Debray[c], Pascale Armand[a]

[a] ICGM, CNRS-UM-ENSCM, UMR 5253, Université Montpellier, Place Eugène Bataillon, 34095 Montpellier Cedex 5, France

[b] Institut Charles Coulomb, Université Montpellier, Place Eugène Bataillon, 34095 Montpellier Cedex 5, France

[c] Univ. Grenoble Alpes, CNRS, Grenoble INP, Institut Néel, 38000 Grenoble, France

E-mail: Philippe.Papet@univ-montp2.fr

Abstract:

The temperature-dependence of the piezoelectric properties of trigonal α-GeO_2 single-crystals obtained by the high-temperature flux method was measured by the resonance technique of the electrical impedance in the 20°C - 600°C range. To approach the values of the two independent piezoelectric coefficients d_{11} and d_{14}, we first measured as a function of temperature the elastic coefficients S_{11}, S_{14} and S_{66} and the dielectric permittivity ε_{11}which are involved in the coupling coefficient k of both the thickness shear mode and the transverse mode. A Y-cut plate with a simple +45°-rotation ((YXtwl) +45°/0°/0°) was used to measure the coupling coefficient of the thickness shear mode, and two X-turned plates ((XYtwl) +45°/0°/0° and (XYtwl) -45°/0°/0°) were prepared to characterize the coupling coefficient of two transverse modes. From the whole experimental measurements, the piezoelectric coefficients of α-GeO_2 were calculated up to 600 °C. They show that this crystal is one of the most efficient in regard of the α-quartz-like family at room temperature, and that its thermal comportment retains large piezoelectric properties up to 600°C.

1. Introduction

Piezoelectric materials are extensively used as sensors or actuators in a wide range of applications involving the measurement of stresses / strains, the energy conversion, the generation and detection of ultrasonic waves, etc. Today, there is a strong demand for piezoelectric materials with improved performances or tailored properties for high temperature applications. For instance, α-quartz, langasite ($La_3Ga_5SiO_{14}$) and α-$GaPO_4$ have been widely investigated for Surface Acoustic Waves/Bulk Acoustic Waves high temperature sensor applications (for high temperature pressure, mass and chemical/gas measurements) [1]. This implies to dispose of materials having a large thermal stability of dielectric and piezoelectric properties. Moreover, for resonant frequency-based sensor devices, such as SAW/BAW resonators, the knowledge of frequency temperature characteristics is important. In addition, a high mechanical quality factor Q_M at an elevated temperature is required to improve sensitivity.

The use of a piezoelectric material at elevated temperature presents many challenges such as possible phase transition, chemical degradation or structural defect propagation which can cancel or lead to thermal instability of the dielectric, piezoelectric and electromechanical coupling constants. For these reasons, the development of lead-free and environmental-safe non centrosymmetric materials with both a high thermal stability and valuable physical properties is challenging.

In the α-quartz-like family, space group $P3_121$ or $P3_221$, with TO_2 (T = Si, Ge) and MXO_4 (M = B, Al, Ga, Fe, Mn; X = P, As) compounds, the piezoelectric coupling factor k strongly depends on the

structural distortion. It has been shown that one of the most distorted and thus, most promising piezoelectric material, would be α-GeO_2 [3-6]. The single crystal growth of α-GeO_2 was already reported by using the low-temperature hydrothermal method in aqueous solutions from a quartz seed [5-7]. These hydrothermally-grown crystals present a phase transition to the stable tetragonal polymorph at around 180°C due to the presence of OH groups in the as-grown crystal which act as a catalyzer [5,7,8]. The growth of α-GeO_2 single crystal at high temperature by the flux method [9-12], is a growth method which avoids the presence of OH impurity in the crystal structure [13] giving rise to α-quartz-structure GeO_2 single crystals without phase transition up to their melting 1116°C [12]. This was already explained by their high crystalline quality [14] and by the low degree of dynamical disorder at high temperature originating from the absence of libration mode of the GeO_4 tetrahedra [15].

In this study, oriented plates were obtained from high-quality flux-grown α-GeO_2 crystals and the high-temperature dependence of the dielectric, piezoelectric and electromechanical coupling constants were measured. This paper reports on the first set of piezoelectric constants of OH-free α-GeO_2 single crystal from room temperature to 600°C.

2. Experimental procedure

Colorless, high-transparent and large-size right-handed single crystals of the non-centrosymetric phase of GeO_2 were grown from a high temperature solution. Details on the experimental crystal growth conditions were already published [11].

Using a Cartesian coordinate system, plates cut perpendicular to $[2\bar{1}0]$, $[010]$ and $[001]$ directions are known as X, Y, and Z cuts respectively, with the center of the plate at the origin. The Z axis of the coordinate system coincides with the natural *c* axis of the crystal. All experimental dielectric and piezoelectric measurements were performed on simple rotated plates. We used the IEEE system of notation for designating the orientation of crystalline plates [18]. By convention, for a simple rotation, the rotational symbol uses as a starting reference one of three hypothetical plates with thickness along *X, Y,* or *Z,* and then carries this plate through simple rotation about coordinate axes, fixed in the reference plate, to reach the final orientation. The notation *l, w, t* (length, width, and thickness of the plate) denotes the orthogonal coordinate axes fixed in the reference plate. By convention the first letter (*X, Y,* or *Z*) indicates the initial principal direction of the thickness of the hypothetical plate and the second letter (*X, Y,* or *Z*) indicates the initial principal direction of the length of the hypothetical plate. The third letter (*l, w,* or *t*) denotes which of the three orthogonal coordinate axes in the hypothetical plate is the axis of the rotation.

The sound velocity υ translating in the α-GeO_2 single crystal in function of the crystallographic orientations was obtained through the Brillouin shift $\Delta\nu_B$ registered at λ= 514.5 nm in the [20°C-600°C] temperature (T) range with a backscattering geometry. The temperature of the samples was regulated with a stability of ±1 °C. Detailed information on the Brillouin instrumental setup was already published [16].

The elastic compliance constants S^E(T) were calculated from the measured elastic stiffness coefficients C^E(T) through the relationship (matrix form), given in Eq. (1).

$$C^E(T)*S^E(T) = 1 \quad (1)$$

An electrically driven mechanical resonance can be created in piezoelectric materials of fixed geometry depending on the boundary conditions [17]. Even if 5 fundamental vibration modes, characterized by an electromechanical coupling factor *k*, exist in crystals belonging to the crystal class

(32), the measurements of only two suitable modes are enough to get the non-zero piezoelectric constants d_{11} and d_{14}.. From the measurements of the temperature-dependent frequencies f_r and f_{aR} of the impedance using the resonance method, the evolution with the temperature of a given electromechanical coupling factor can be obtained. For a lossless resonator the frequency f_r, commonly identified as the resonance frequency, is defined as the frequency of maximum admittance (minimum impedance). The upper frequency f_{aR} is defined as the frequency of maximum impedance (minimum admittance) and is called the antiresonance frequency.

In this work, we have chosen, according to the IEEE standard [18], to measure:

- the coupling factor k'_{26} of shear thickness vibration mode with Eq. (2) [18] using a simple-rotated plate (YXt)+45° (counterclockwise rotation of 45° along Y axis, thickness t = 0.78 mm, length l = 5.9 mm, width w = 3.05 mm).

$$k'^2_{26} = \left(\frac{\pi}{2} * \frac{f_{aR}}{f_R}\right) * \tan\left(\frac{\pi}{2} * \frac{f_{aR}-f_R}{f_{aR}}\right) \quad (2)$$

- the coupling factor k'_{12} of extensional mode using Eq. (3) [18] with two simple-rotated plates, one (XYt)+45° (l = 5.68 mm, w = 1.78 mm and t = 0.58 mm) to get $k'^{(a)}_{12}$ and one (XYt)-45° (l = 4.70 mm, w = 1.47 mm and t = 0.36 mm) to get $k'^{(b)}_{12}$.

$$\frac{f_{aR}-f_R}{f_R} = 4\frac{(k'^{(a,b)}_{12})^2}{\pi^2} \quad (3)$$

In a rotated coordinate system all dielectric, elastic and coupling constants are noted with an apostrophe (′) while the corresponding constants measured in the original coordinate system do not have one. The choice of using a Y rotated plate instead of a Y-cut was due to the size of the as-grown single crystal. Indeed, to respect the boundary conditions for the resonance method it was easier to use a simple-rotated plate (YXt)+ 45°. In order to calculate the d_{14} piezoelectric constant (see section 3.3), two X rotated plates were necessary.

For these three simple-rotated plates, the two large faces perpendicular to the Y (X) axis were covered with a 20 nm thick layer of Pt metal, deposited by sputtering, which served as electrodes. The exciting electric field was applied along the Y (X) axis (parallel to the thickness) and f_r and f_{aR} frequencies were measured with an Agilent HP 4294A impedance phase analyzer.

The temperature-dependent impedance measurements were carried out with plates connected by Pt wires in a dense alumina cell placed vertically in a furnace. Even if the α-GeO_2 material is stable up to 1100°C [12], it has been decided to perform measurements only up to 600 °C to ensure the reliability of the measurements. Even if no visible degradation of the electrodes, cracks or peeling off, was observed, Secondary Ions Mass Spectroscopy measurements were performed on samples heated at 600°C for 48 hours in the air and have shown a Pt diffusion in GeO_2 up to a 1µm-depth from the electrode surfaces..

The mechanically-free dielectric permittivity ε^X_{11} was obtained by measuring, in the 20°C-600°C temperature range, the capacitance C at low frequency (1 kHz) of the (XYt)+45° and (YXt)+45° plates covered with electrodes because they had suitable boundary conditions to measure $\varepsilon^X_{11}(T) = \varepsilon^X_{22}(T)$ [17-19].

3. Results

3.1 Elastic constants

The Brillouin shift was registered on non-metalized X-cut and Y-cut plates. The high temperature evolution of the elastic moduli at constant electric field (electrically free) $s_{44}^{E}(T)$, $|S_{14}{}^{E}|$(T) and s_{66}^{E}(T) are reported in Fig.1.

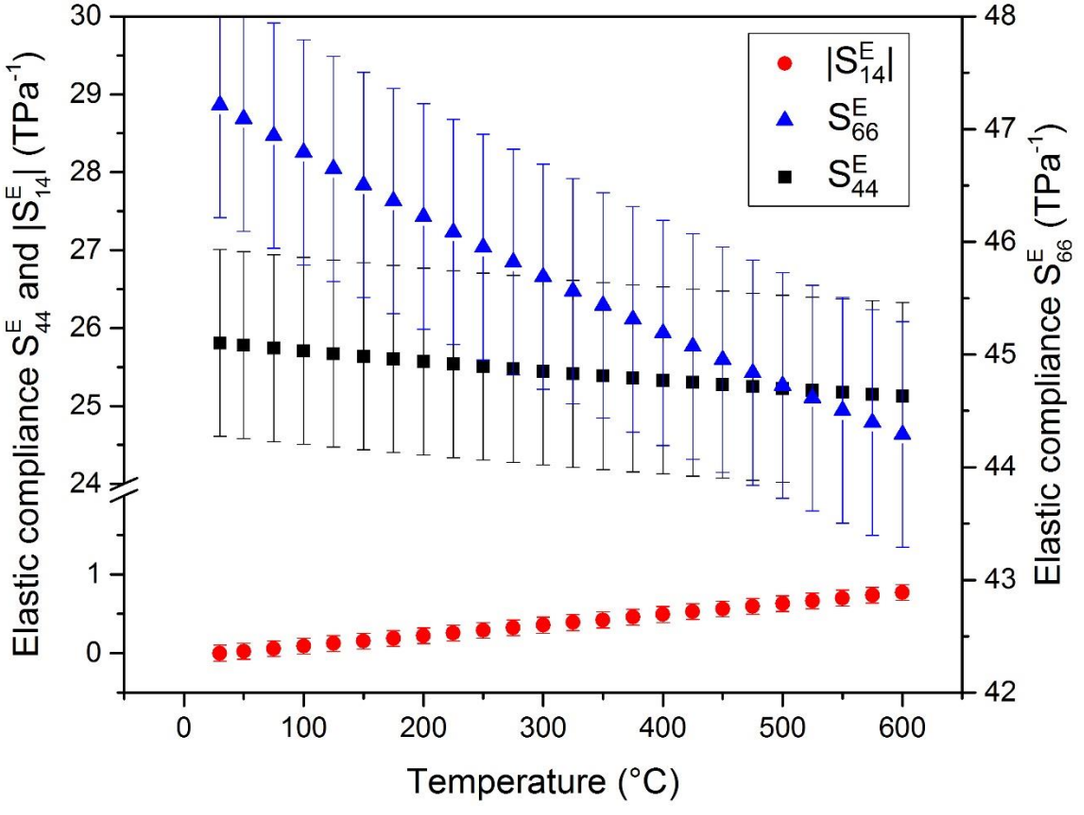

Fig. 1. Thermal evolution of the elastic compliances $S_{66}{}^{E}$, $S_{44}{}^{E}$ and $|S_{14}{}^{E}|$. The error bars are the standard deviations (close to 1 for $S_{66}{}^{E}$, 1.2 for $S_{44}{}^{E}$ and 0.1 for $|S_{14}{}^{E}|$).

3.2 Dielectric properties

The average of the measured values of the mechanically-free ε_{11}^{X}(at 1 kHz) permittivity and the dielectric loss versus the temperature is reported in Fig. 2. The large error bars of the data measured are due to the weak accuracy of this method of measurement even if we respect the boundary conditions for the geometry of plates.

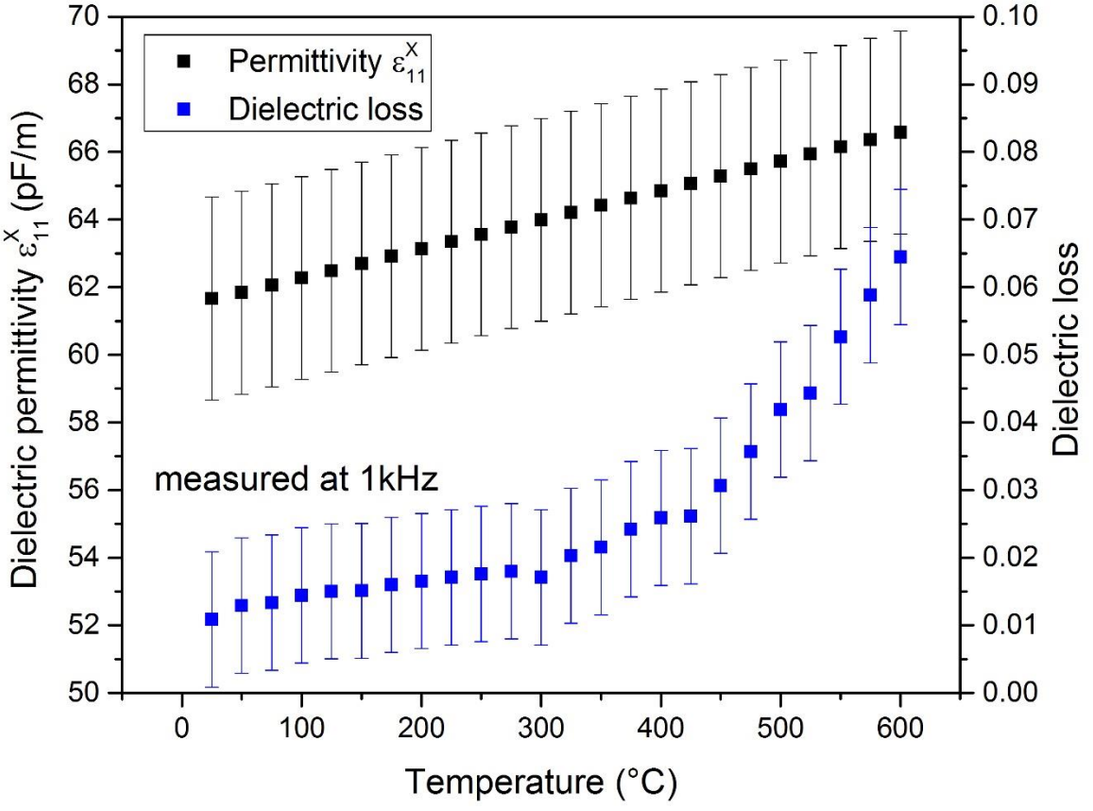

Fig. 2. Mechanically-free ε_{11}^{X} permittivity and Dielectric Loss depending on the temperature (measured at 1kHz). The points represent the average of five measures at each temperature and the error bars are the standard deviation (close to 3 pF/m for ε_{11}^{X} and 0.01 for Dielectric Loss).

3.3 Piezoelectric properties

- *d_{11} according to the temperature*

In the rotated coordinate system, the coupling factor k'_{26} of shear thickness vibration mode is given by Eq. (4).

$$k'_{26} = \frac{d'_{26}}{\sqrt{s'^{E}_{66}\varepsilon'^{X}_{22}}} \tag{4}$$

Knowing the elastic constants s^{E}_{66} and the permittivity ε^{X}_{22}, we have to compute s'^{E}_{66} and ε'^{X}_{22} and d'_{26} using the transformation law for a tensor of rank 4 (elastic coefficients), rank 3 (piezoelectric coefficients) and rank 2 (permittivity tensor). The new relations are given in Eq. (5).

$$\varepsilon'_{22} = \varepsilon_{22} = \varepsilon_{11} \tag{5a}$$

$$s'_{66} = (s_{66}\cos^2\theta + s_{44}\sin^2\theta) \quad (5b)$$

$$d'_{26} = 2d'_{212} = 2\cos\theta\, d_{212} = \cos\theta\, d_{26} \quad (5c)$$

Finally, we obtain Eq. (6).

$$k'_{26}(T) = \frac{d'_{26}(T)}{\sqrt{s'^{E}_{66}(T)\varepsilon'^{X}_{22}(T)}} = \frac{d_{26}(T)\cos\theta}{\sqrt{(s^{E}_{66}(T)\cos^2\theta + s^{E}_{44}(T)\sin^2\theta)\varepsilon^{X}_{11}(T)}} \quad (6)$$

Fig. 3a reports the measures of the electromechanical coupling coefficient k'_{26} by the resonance method depending on the temperature for a (*YXt*)+ 45° plate.

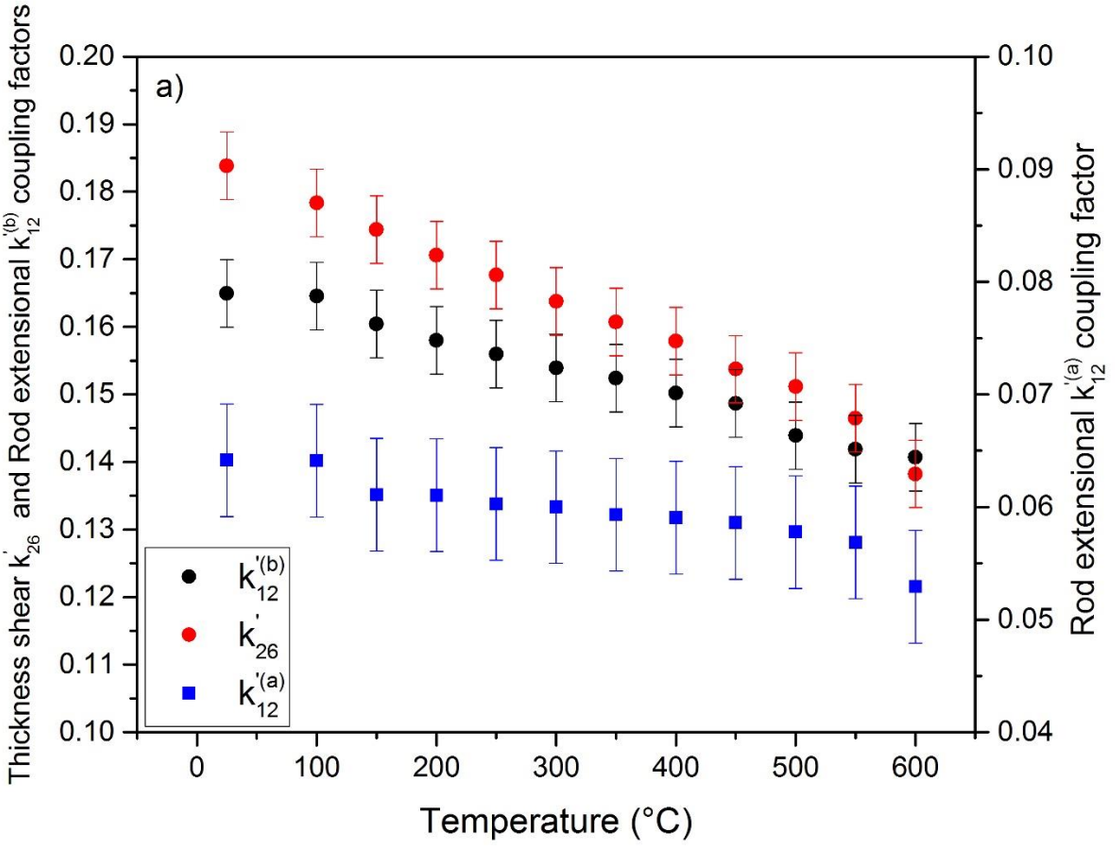

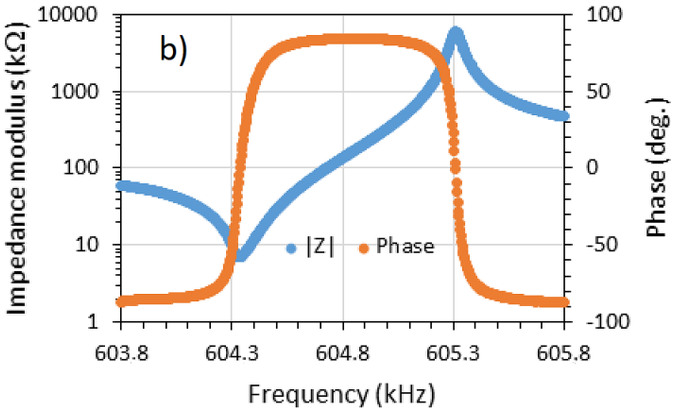

Fig. 3 (a) Thickness shear k'_{26} and rod extensional $k_{12}^{\prime(a)}$ and $k_{12}^{\prime(b)}$ coupling factors in the 20-600°C temperature range (each point represents the average of five measures and the error bars are the standard deviation (close to 0.005)) and (b) room temperature impedance modulus and phase near resonance for the (*XYt*)+45° plate.

As $d_{26} = -2d_{11}$ [18], the thermal evolution of the d_{11}(T) piezoelectric coefficient, obtained from the measured elastic compliances $s_{44}^{E}(T)$ and s_{66}^{E}(T) (Fig. 1), dielectric permittivity $\varepsilon_{11}^{X}(T)$ (Fig. 2) and electromechanical coupling coefficients $k'_{26}(T)$ (Fig. 3), is shown in Fig. 4.

- *d_{14} according to the temperature*

Direct measurement of the piezoelectric strain constant d_{14} is not easy to perform because it only appears for shear face vibration mode in X- or Y-cut plates. Nevertheless, it is possible to measure a vibration mode, such as an extensional one, using a X-cut plate rotated along the X axis and electrically driven with $\vec{E}//$ to the X axis. The electromechanical coupling factor k'_{12} for plate extensional mode in the rotated coordinate system is given by Eq. (7).

$$(k'_{12})^2 = \frac{(d'_{12})^2}{s_{22}^{\prime E} * \varepsilon_{11}^{\prime X}} \tag{7}$$

The new relations are given in Eq. (8) for a simple-rotated plate (*XYt*)+θ°.

$$\varepsilon'_{11} = \varepsilon_{11} \tag{8a}$$

$$s'_{22} = (s_{11}\cos^4\theta + s_{44}\sin^2\theta\cos^2\theta + 2s_{13}\sin^2\theta\cos^2\theta - 2s_{14}\sin\theta\cos^3\theta + s_{33}\sin^4\theta) \tag{8b}$$

$$d'_{12} = d'_{122} = \cos^2\theta\, d_{12} + \cos\theta\sin\theta\, d_{14} = -\cos^2\theta\, d_{11} + \cos\theta\sin\theta\, d_{14} \tag{8c}$$

Finally, we obtain Eq. (9).

Journal of Applied Physics

$$k'_{12} = \frac{-\cos^2\theta d_{11} + \cos\theta \sin\theta d_{14}}{\sqrt{\left(s^E_{11}\cos^4\theta + s^E_{44}\sin^2\theta\cos^2\theta + 2s^E_{13}\sin^2\theta\cos^2\theta - 2s^E_{14}\sin\theta\cos^3\theta + s^E_{33}\sin^4\theta\right)\varepsilon^X_{11}}} \quad (9)$$

Thus, by measuring the coupling factor of the transverse vibration mode of two simple-rotated (XYt)+45° and (XYt)-45° plates and, knowing the d_{11} values measured with the Y-cut rotated plate (see Fig. 4), we can calculate the value of d_{14} [19-20]. Indeed, if $\theta = +45°$, $k'^{(a)}_{12}$is given by Eq. (10a) and if $\theta = -45°$, $k'^{(b)}_{12}$ is given by Eq. (10b).

$$k'^{(a)}_{12}(T) = \frac{-d_{11}(T) + d_{14}(T)}{\sqrt{\left(s^E_{11}(T) + s^E_{44}(T) + 2s^E_{13}(T) - 2s^E_{14}(T) + s^E_{33}(T)\right)\varepsilon^X_{11}(T)}} \quad (10a)$$

$$k'^{(b)}_{12}(T) = \frac{-d_{11}(T) - d_{14}(T)}{\sqrt{\left(s^E_{11}(T) + s^E_{44}(T) + 2s^E_{13}(T) + 2s^E_{14}(T) + s^E_{33}(T)\right)\varepsilon^X_{11}(T)}} \quad (10b)$$

Since $|S_{14}{}^E|(T)$ with $20°C \leq T \leq 600°C$ is almost two orders of magnitude lower than $s^E_{44}(T)$, see Fig. 1, we can assume that $d_{14}(T)$ follows Eq. (11) in the temperature range of measurements.

$$d_{14}(T) \approx d_{11}(T) \times \frac{\left(1 - \frac{k'^{(a)}_{12}(T)}{k'^{(b)}_{12}(T)}\right)}{\left(1 + \frac{k'^{(a)}_{12}(T)}{k'^{(b)}_{12}(T)}\right)} \quad (11)$$

The temperature dependence of $k'^{(a)}_{12}$ and $k'^{(b)}_{12}$ is reported in Fig. 3a, and the deduced values of $d_{14}(T)$ can be seen in Fig. 4.

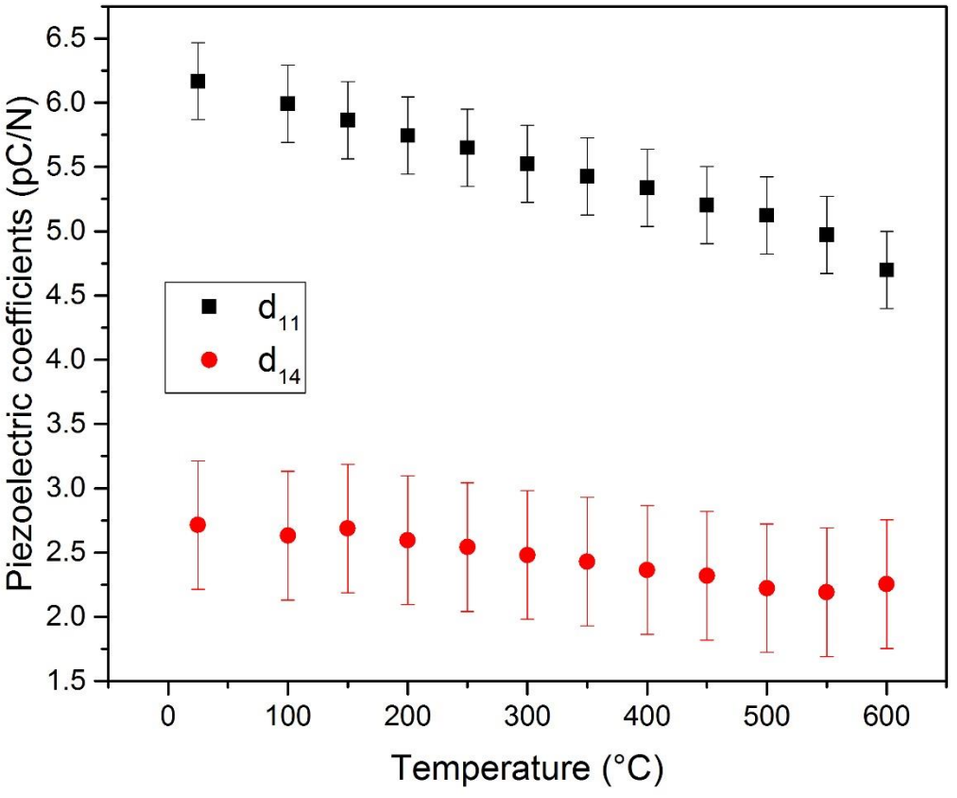

Fig. 4. Temperature dependence of the piezoelectric strain constants d_{11} and d_{14}. The error bars are the standard deviation (close to 0.3 pC/N for d_{11} and 0.5 pC/N for d_{14}).

4. Discussion

4.1 Room-temperature characterizations

Table 1 presents the room-temperature parameters measured in this study compared to experimental and calculated values found in literature.

Table 1
Calculated and room-temperature measured parameters for α-GeO_2 single crystal.

	This work	Experimental results	Theoretical results
$\lvert S_{14}^E \rvert$ (TPa^{-1})	≈ 0.00 ± 0.03	1.29 [21]	2.60 [22]
S_{44}^E (TPa^{-1})	25.8 ± 0.6	27.17 [21]	30.20 [22]
S_{66}^E (TPa^{-1})	47 ± 2	47.87 [21]	55.54 [22]
ε_{11}^X ($pF.m^{-1}$)	61± 5	48.00 [16] 65.78 [21]	45.25 [22] 53.12 [23]
d_{11}($pC.N^{-1}$)	6.2 ± 0.4	5.70 [16]	6.31 [22]

Journal of Applied Physics

AIP Publishing

		4.10 [21]	6.00 [6]
d_{14}(pC.N^{-1})	2.7 ± 0.5	3.82 [21]	3.11 [22]

Concerning the elastic constants, we quite agree with the published values except for the S_{14}^{E} constant for which our value is close to zero.

Our room-temperature d_{11} and d_{14} piezoelectric strain constants are close to the theoretical ones and the low d_{11} and the high d_{14} experimental values reported in published articles were obtained from plates of α-GeO_2 synthesized by hydrothermal process which contains a notable concentration of OH group (d_{11} = 4.04 and d_{14} = 3.82 pC/N [21]).

In Table 2, room temperature experimental piezoelectric constants for single crystals belonging to the α-quartz family are reported. As it can be seen, α-GeO_2 exhibits the highest values of the piezoelectric parameters as it was predicted based on the degree of crystal structure distortion in the α-quartz family [3-6].

Table 2

Comparison of the experimental piezoelectric parameters in the α-quartz family single crystals (Langasite $La_3Ga_5SiO_{14}$ belongs to the trigonal system, point group *32*).

	α-SiO_2 [25]	α-$AlPO_4$ [4]	α-$GaPO_4$ [4]	α-GeO_2	$La_3Ga_5SiO_{14}$ [28]
d_{11} (pC.N^{-1})	2.31	3.30	4.50	6.2 ± 0.3	6.15
d_{14} (pC.N^{-1})	0.73	1.62	1.94	2.7 ± 0.5	-

4.2 Temperature dependence of the elastic, dielectric and piezoelectric properties

The dielectric permittivity is stable in the 20-600°C temperature range and the slight enhancement of the dielectric permittivity with temperature observed in Fig. 2 may be explained by an increase of the mobility of charged defects/impurities present in the material. The thermal activation of the mobility of charged defects may improve the contribution of the space charge polarization (induced by defects) to the dielectric permittivity. However, this phenomenon, observed in many inorganic materials with a low dielectric permittivity[17], is small for α-GeO_2 for temperatures under 600°C (the slope of the linear curve is 8.61*10^{-4} F.m^{-1}.C^{-1}).

The coupling coefficient $k'_{26}(T)$ and $k'_{12}(T)$, which are nondimensional coefficients useful for the description of a piezoelectric material under a particular stress and electric field configuration for conversion of stored energy to mechanical or electric work[18], decrease when the temperature increases. However, we must avoid attributing all the behaviour of piezoelectric coupling coefficients, in the temperature range explored, Fig. 4, only to the resonator. By using thin films of platinum for electrodes, some degradation phenomena as a result of agglomeration, recrystallization, and dewetting effects can be observed at high temperatures [25] and can lead to partial loss of thin film's electrical conductivity [26-27]. Moreover, the resonator is placed between a plate of platinum that ensures the electrical contact with the lower electrode and a platinum wire in contact with the upper electrode. If, at high temperature there is a bad adhesion between the plate and the electrode, capacitive effects may appear. To take into account all the parasitic effects due to the experimental measurement system, a serial impedance R_{el}-C_{el} branch in series with the equivalent circuit (near the resonance) of the

resonator can be used, with R_{el} and C_{el} respectively the resistance and the capacitance of experimental measuring system (Pt plates, wires and electrodes). For ideal lossless materials, the resonator impedance is purely reactive, and the characteristic frequencies of a vibration mode coincide with the minimum and maximum of the impedance [18]. Adding a branch in series to the equivalent circuit allows to underline the likely effects of experimental measurements system at high temperatures onto the impedance data. Indeed, introduction of C_{el} term in the reactive expression of impedance could lead to small change in the characteristic frequencies at high temperature.

The piezoelectric constant d_{14} seems to be less sensitive to temperature in the studied temperature range, Fig. 4. However, the accuracy of d_{14} values is less reliable than the d_{11} one because we had to use the d_{11} data modulated by the ratio of coupling coefficients of two rotated X plates experimentally measured in order to calculate d_{14}.

5. Conclusion

α-GeO_2 crystal structure is of the same crystal class (32) as α-quartz, which is the piezoelectric single crystal of reference. At room temperature, this material is largely more efficient than α-quartz with piezoelectric coefficients 3 times higher. In addition, piezoelectric properties are preserved when subjecting the α-GeO_2 material to high temperatures. The measurements, by the resonant method on oriented α-GeO_2 plates, of the electromechanical coupling factors depending on the temperature, allowed us to highlight that this material is still piezoelectric at 600°C with high values of piezoelectric coefficients d_{11} and d_{14}. The decreases of d_{11}, and to a lesser extent the one of d_{14}, when the temperature is increased, consider the intrinsic behaviour of the material, but also the likely evolution of electrical contacts (wires and electrodes).

This first high-temperature characterization of the piezoelectric performance of the α-GeO_2 single crystal shows that this lead-free material, due to its thermal stability of both its structure and its piezoelectric constants, is a good candidate for high temperature piezoelectric applications.

Acknowledgements.

This work has been done with the financial support of the French National Agency ANR (contract 14-CE07-0017)

References

1 M.V. hamidon, V. Skarda, N.M. White, F. Krispel, P. Krempl, M. Binhack and W.Buff, Sens. Actuators, A 123-124, 403 (2005).

2 S. Zhang, and F. Yu, J. Am. Ceramic Society 94(10), 3153 (2011).

3 E. Philippot, A. Goiffon, A. Ibanez, and M. Pintard, J. Solid State Chem. 110, 356 (1994).

4 E. Philippot, D. Palmier, M. Pintard, and A. Goiffon, J. Solid State Chem. 123,1 (1996).

5 D.V. Balitsky, V.S.Valitsky, Y.V. Pisarevley, E. Philippot, O.Y Silvestrova, and D.Y Pushcharovsky, Ann. Chim. Sci. Mat, 26, 183 (2001).

6 P.W. Krempl, J. Phys. IV France 126, 95 (2005).

7 R. Roy, and S. Theokritoff, J. Crystal Growth, 12, 69 (1972).

8 L.N. Demianets, Prog. Crystal Growth and Charact., 21, 299 (1990).

9 C.B. Finch, and G.W Clark, Am. Mineral., 53, 1394 (1968).

10 J.W. Goodrum, J. Cryst. Growth 13/14, 604 (1972).

11 A. Lignie, B. Ménaert, P. Armand, A. Peña, J. Debray, and P. Papet, Cryst. Growth Des. 13, 4220 (2013).

12 P. Armand, A. Lignie, M. Beaurain and P. Papet, Crystals 4, 168 (2014).

13 A. Lignie, P. Armand and P. Papet, Inorg. Chem. 50, 9311 (2011).

14 A. Lignie, D. Granier, P. Armand, J. Haines and P. Papet, J. Appl. Cryst. 45, 272 (2012).

15 G. Fraysse, A. Lignie, P. Hermet, P. Armand, D. Bourgogne, J. Haines, B. Ménaert and P. Papet, Inorg. Chem. 52, 7271 (2013).

16 A. Lignie, W. Zhou, P. Armand, B. Rufflé, R. Mayet, J. Debray, P. Hermet, B. Ménaert, P. Thomas, and P. Papet, ChemPhysChem 15, 118 (2014).

17 R.E. Newnham, Properties of materials, anisotropy, symmetry, structure, Oxford University Press (2005).

18 IEEE Standard on Piezoelectricity, IEEE/ANSI Std. 176 (1987).

19 W. G. Cady, Piezoelectricity, McGraw-Hill, New York (1946).

20 A.C. Lynch, Proc. Phys. Soc. B 63, 890 (1950).

21 D.V. Balitsky, V.S.Valitsky, Yu.V. Pisarevsky, E. Philippot, O.Yu. Silvestrova and D.Yu. Pisharovsky, Ann. Chim. Sci. Mat., 26, 183 (2001).

22 Kh. E. El-Kelany, A. Erba, P. Carbonnière and M. Rérat, J. Phys. Condens. Matter 26, 205401 (2014).

23 E. Ghobadi, J.A. Capobianco, Phys. Chem. Chem. Phys. 2, 5761 (2000).

24 R. Bechmann, Phys. Rev. 110, 1060 (1958).

25 D. Frankel, G. Bernhardt, B. Sturtevant, T. Moonlight, M. Pereira da Cunha, R.S Lad, In Proceedings of the IEEE Sensors, Lecce, Italy, 82 (2008)

26 D. Richter, S. Sakharov, E. Forsén, E. Mayer, L. Reindl, S. Fritze, Procedia Eng. 25, 168 (2011).

27 S.L. Firebaugh, K.F. Jensen, M.A. Schmidt, J. Microelectromech. Syst. 7, 128 (1998).

28 J. Bohm, E. Chilla, C. Flannery, H.J. Frohlich, T. Hauke, R.B. Heimann, M. Hengst, and U. Straube, J. Cryst. Growth, 216, 293 (2000).

Journal of Applied Physics

PLEASE CITE THIS ARTICLE AS DOI: 10.1063/1.5116026

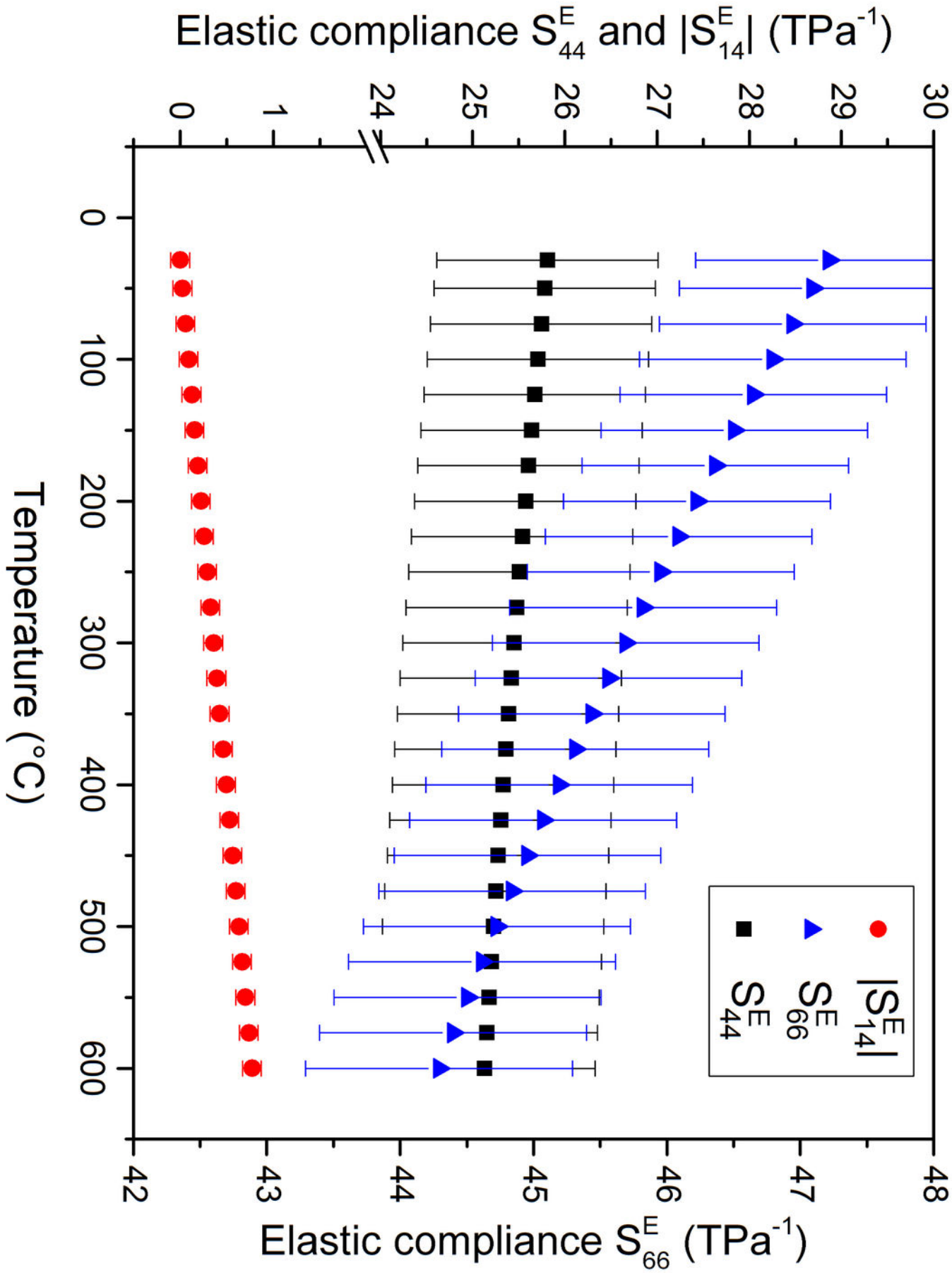

AIP Publishing

Journal of Applied Physics

ACCEPTED MANUSCRIPT

This is the author's peer reviewed, accepted manuscript. However, the online version of record will be different from this version once it has been copyedited and typeset.
PLEASE CITE THIS ARTICLE AS DOI: 10.1063/1.5116026

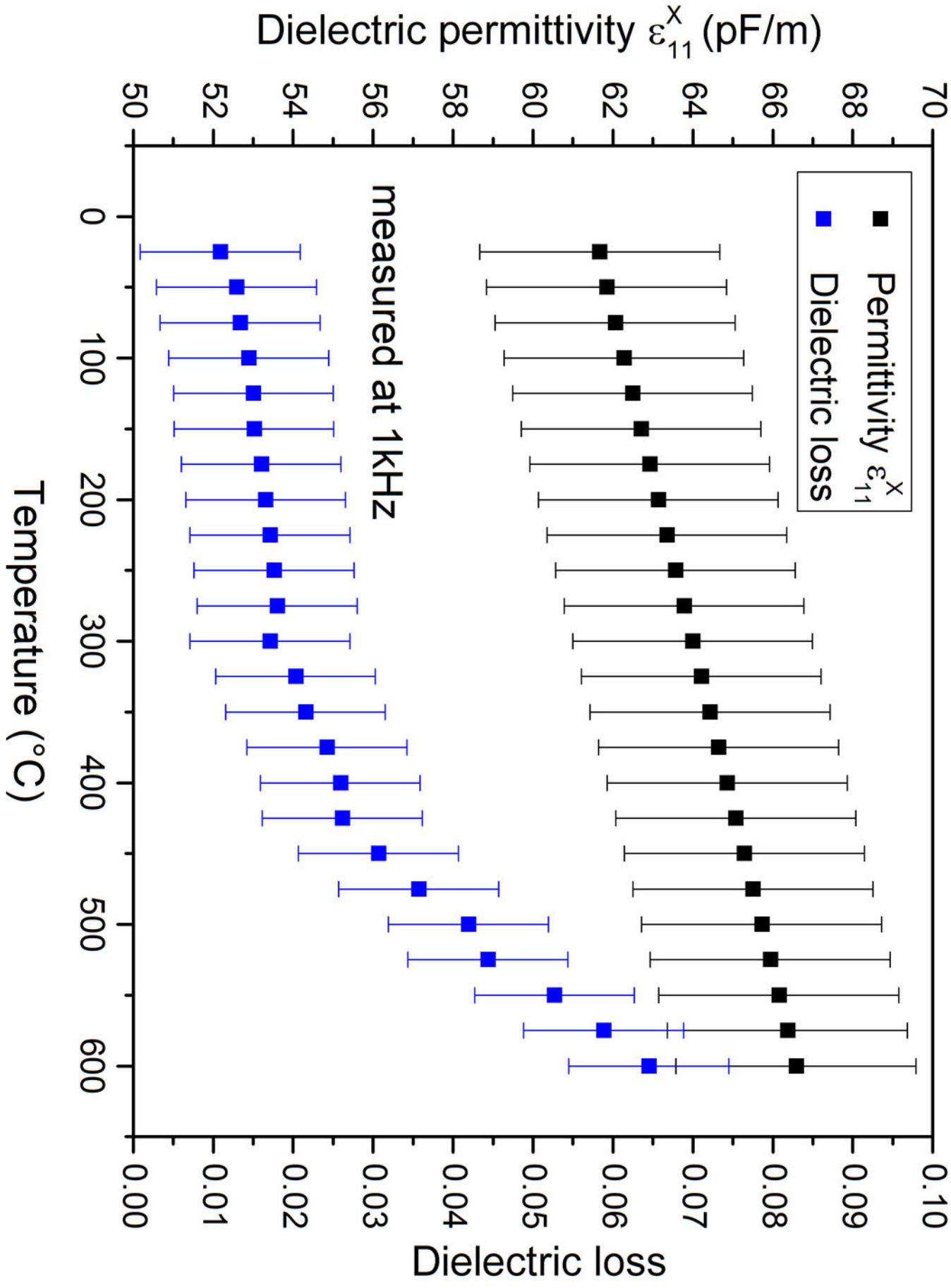

AIP Publishing

Journal of Applied Physics

ACCEPTED MANUSCRIPT

This is the author's peer reviewed, accepted manuscript. However, the online version of record will be different from this version once it has been copyedited and typeset.
PLEASE CITE THIS ARTICLE AS DOI: 10.1063/1.5116026

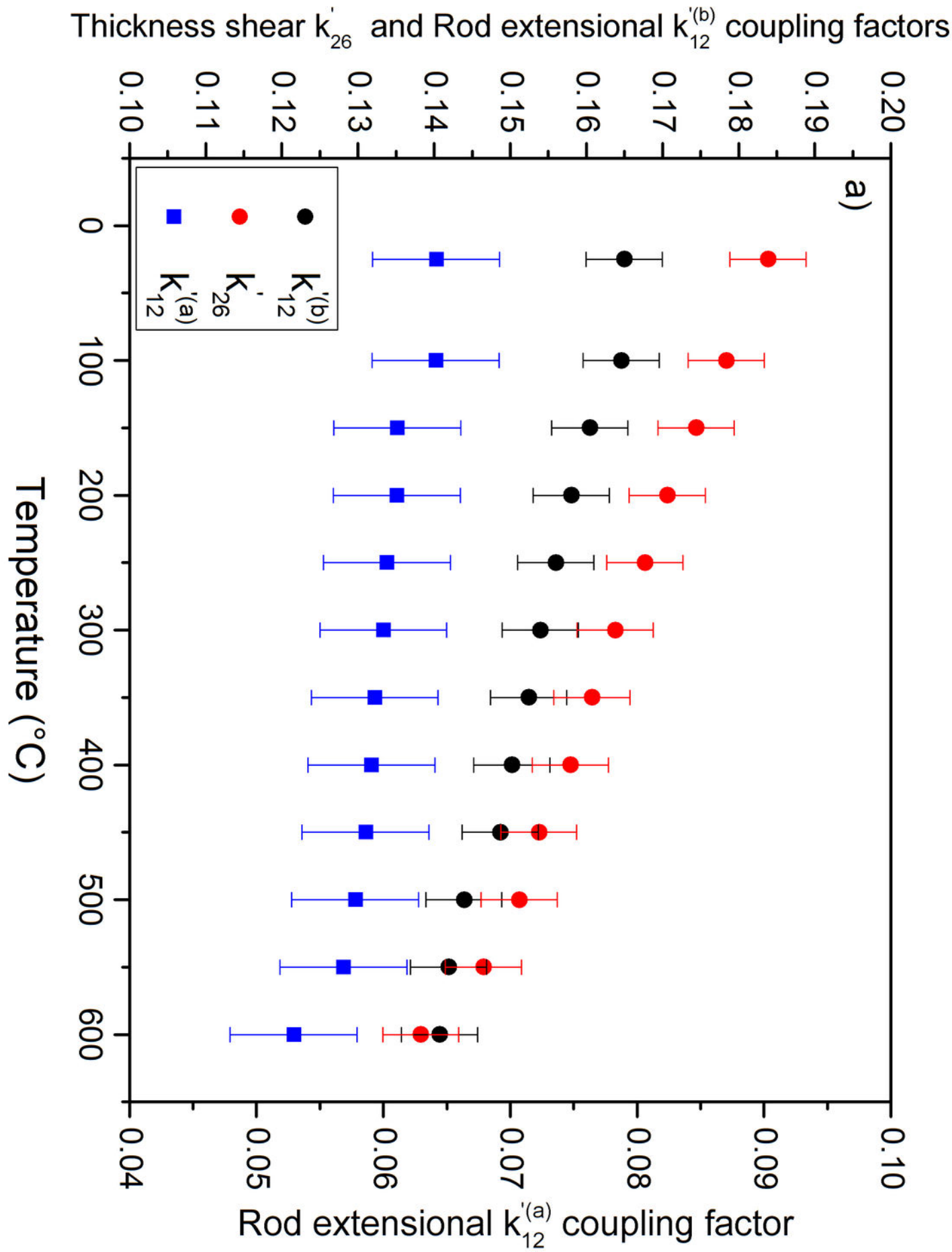

Journal of Applied Physics

PLEASE CITE THIS ARTICLE AS DOI: 10.1063/1.5116026

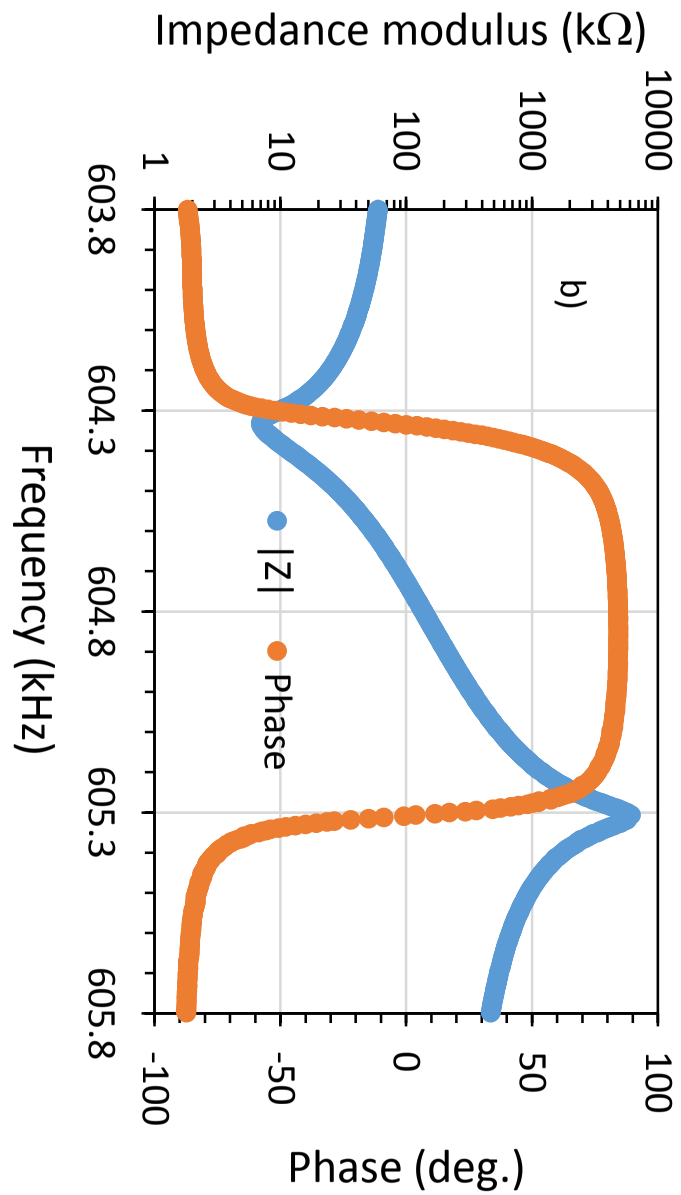

AIP Publishing

Journal of Applied Physics

ACCEPTED MANUSCRIPT

This is the author's peer reviewed, accepted manuscript. However, the online version of record will be different from this version once it has been copyedited and typeset.
PLEASE CITE THIS ARTICLE AS DOI: 10.1063/1.5116026